العددِ 20 شباط 2026
No.20 Feb.2026
المجلة العراقية للبحوث الانسانية والاجتماعية والعلمية
Iraqi Journal of Humanitarian, Social and Scientific Research
Print ISSN 2710-0952 Electronic ISSN2790-1254

التحليل التجريبي والعددي لتأثير أشكال دبوس الأداة في اللحام بالاحتكاك التحريكي للمواد المتباينة

حسين عبد الزهره حسن الوزني

تخصص الإنتاج والتصنيع ، مديرية مجاري كربلاء المقدسة, كربلاء , العراق

husseinalwazny3275@gmail.com

المستخلص

تتناول هذه الدراسة تحليل التأثير المتكامل لأشكال دبوس الأداة على سلوك تدفق المادة وتوزيع الإجهادات المتبقية أثناء عملية اللحام بالاحتكاك التحريكي (FSW) للمواد الألمنيومية المتباينة، من خلال دمج التحليل العددي باستخدام العناصر المحدودة مع التحقق التجريبي. تم تطوير نموذج حراري–ميكانيكي متقدم لمحاكاة توليد الحرارة الناتجة عن الاحتكاك والتشوه اللدن، إضافة إلى تمثيل تدفق المادة غير النيوتوني حول دبوس الأداة الدوّار، بالاعتماد على نموذج اللزوجة (Carreau–Yasuda) وصياغة مرنة–لدنة للإجهادات. شملت الدراسة مقارنة منهجية لعدة هندسات لدبوس الأداة، بهدف تقييم تأثيرها على توزيع درجات الحرارة، ومعدلات الانفعال، وكفاءة الخلط المادي، وتكوّن الإجهادات المتبقية داخل منطقة اللحام. تم دعم نتائج المحاكاة العددية ببيانات تجريبية مستمدة من الفحوصات المجهرية، وتوزيع الصلادة، واختبارات الشد، مما أتاح تقييمًا واقعيًا لدقة النموذج المقترح. أظهرت النتائج أن الدبابيس متعددة الأضلاع وغير المركزية تؤدي إلى تحسين ملحوظ في فعالية التحريك وتجانس التوزيع الحراري، مع تقليل تركّز الإجهادات المتبقية مقارنة بالدبابيس الأسطوانية التقليدية، وهو ما انعكس إيجابًا على جودة الوصلة وخواصها الميكانيكية. تؤكد هذه الدراسة أن الدمج بين التحليل العددي والتجريب العملي يمثل أداة فعّالة لتوجيه تصميم أدوات اللحام وتحسين معايير عملية اللحام بالاحتكاك التحريكي للمواد المتباينة.

الكلمات المفتاحية: اللحام بالاحتكاك التحريكي، التحليل التجريبي والعددي، تحليل العناصر المحدودة، دبوس الأداة، الإجهادات المتبقية

Experimental and Numerical Analysis of Tool Pin Profiles in Dissimilar Friction Stir Welding

HUSSEIN ABDALZAHRA HASAN ALWAZNI

Employee - Production and Manufacturing Specialization - Karbala Sewerage Directorate - Operations Division – Iraq

husseinalwazny3275@gmail.com

Abstract

This study investigates the combined effect of tool pin profiles on material flow behavior and residual stress distribution during friction stir welding (FSW) of dissimilar aluminum alloys by integrating finite element analysis with experimental validation. An advanced thermo-mechanical model was developed to simulate frictional heat generation, plastic deformation, and non-Newtonian

material flow around the rotating tool pin. The model incorporates the Carreau–Yasuda viscosity law and an elastic–plastic stress formulation to accurately represent material behavior under severe thermo-mechanical loading. A systematic comparison of multiple tool pin geometries was conducted to evaluate their influence on temperature distribution, strain rate evolution, material mixing efficiency, and residual stress formation within the weld zone. Numerical predictions were corroborated with experimental evidence obtained from microstructural examinations, hardness mapping, and tensile testing, enabling a realistic assessment of the model's predictive capability. The results demonstrate that polygonal and eccentric pin profiles significantly enhance stirring efficiency and thermal homogeneity while reducing residual stress concentration compared with conventional cylindrical pins. These improvements translate into superior joint integrity and mechanical performance. The findings confirm that the combined experimental–numerical approach provides a robust framework for understanding process–structure–property relationships and offers practical guidance for optimizing tool design and process parameters in friction stir welding of dissimilar materials.

Keywords: Friction stir welding; Experimental–numerical analysis; Finite element analysis; Tool pin profile; Residual stresses

1. Introduction

Friction stir welding (FSW), developed in 1991 at The Welding Institute (TWI) in the United Kingdom, has become a well-established solid-state joining technique, particularly suited for aluminum alloys due to its ability to produce high-quality joints without melting the base materials. The process relies on severe plastic deformation and frictional heat generated by a rotating tool, resulting in refined microstructures, reduced defect formation, and improved mechanical performance compared with conventional fusion welding methods [1,3].

The quality of friction stir welded joints is strongly governed by tool design—especially the geometry of the pin and shoulder—as well as by process parameters such as rotational speed, traverse speed, and tool tilt angle, all of which directly influence heat generation, material flow behavior, and microstructural evolution within the weld zone [8,10]. Among these factors, tool pin geometry plays a critical role in controlling material stirring, consolidation, and defect suppression, particularly in dissimilar aluminum alloy joints where asymmetric flow behavior is often observed [5,6].

Material flow during FSW has been investigated using a wide range of experimental and numerical approaches, including tracer-based microscopy, physical analogue modeling, and finite element–based thermo-mechanical simulations. These studies have demonstrated characteristic flow patterns around

the rotating pin and have shown that profiled pins, such as square or polygonal geometries, enhance material mixing and grain refinement compared with conventional cylindrical pins [2,11,13]. Numerical simulations further reveal that flat or angular pin features induce localized strain concentration and improved plastic flow, contributing to superior joint integrity [9,14].

Despite these advances, systematic investigations isolating subtle variations in tool pin geometry while maintaining comparable welding conditions remain limited. In particular, the combined influence of pin profile on material flow behavior and residual stress development has not been sufficiently clarified, even though residual stresses significantly affect joint performance and service life [7,15]. This gap is especially pronounced in dissimilar aluminum alloy welds, where complex thermo-mechanical interactions arise [16,17].

Therefore, the present study aims to systematically examine the effect of different tool pin profiles on material flow characteristics and residual stress distribution in friction stir welding of AA6082-T6 aluminum alloys. By integrating finite element–based thermo-mechanical modeling with experimental validation, including microstructural analysis, hardness mapping, and tensile testing, this work seeks to establish a clear process–structure–property relationship. The outcomes are intended to provide practical guidance for optimizing tool design and improving weld quality in friction stir welding of dissimilar materials [9,12,18].

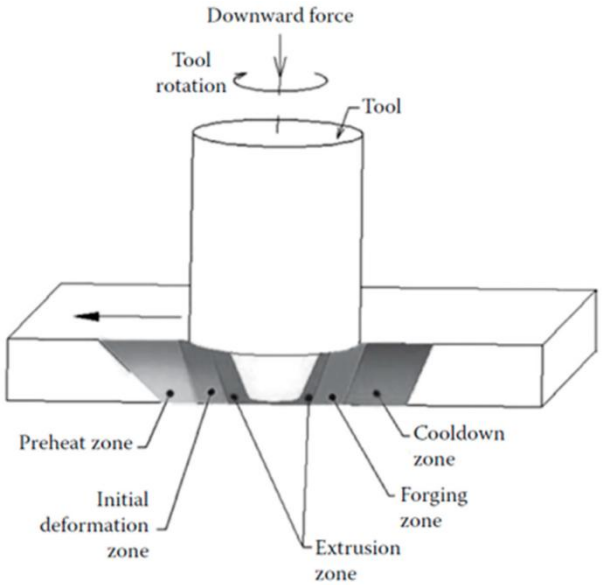

Figure 1. Stages in the Friction Stir Welding (FSW) process

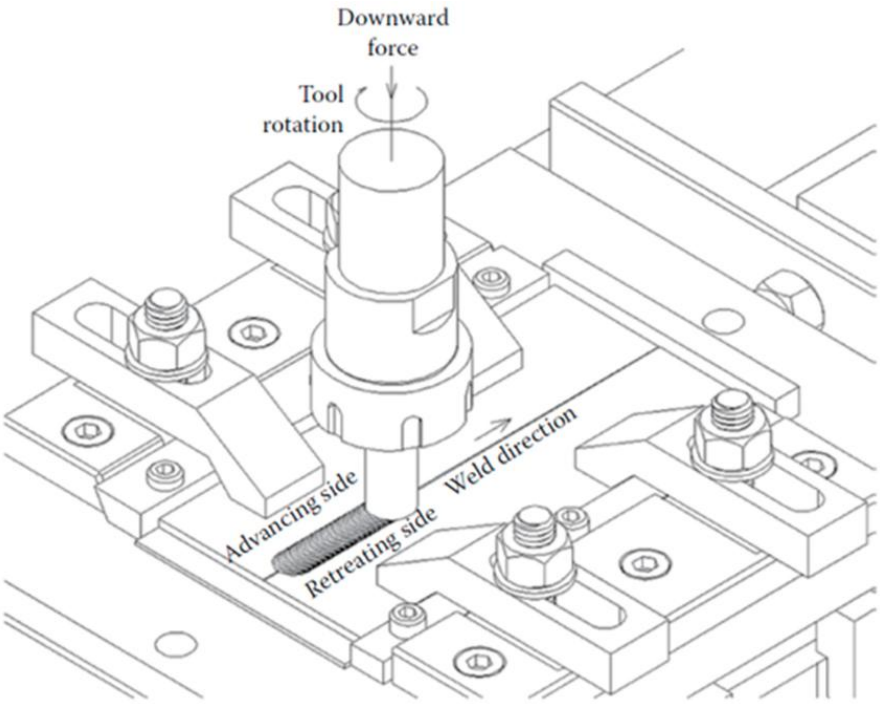

Figure 2. Schematic of FSW process

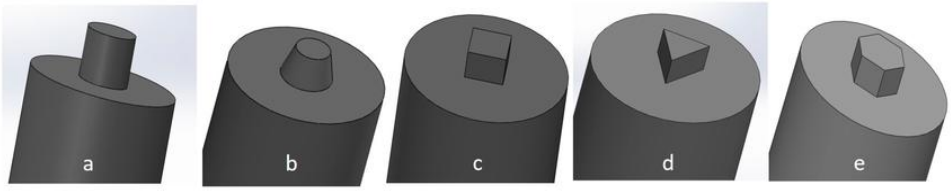

Figure 3. FSW tools with different pin profile (a) cylindrical; (b) tapered cylindrical; (c) triangular; (d) square and (e) hexagonal.

Table .1 Comparison of different tool profiles and their effects on material flow and welding quality.

Tool Pin Profile	Material Flow	Weld Quality	Remarks
Cylindrical	Moderate, symmetrical	Smooth surface, moderate defect rate	Commonly used, but lower stirring effect
Tapered Cylindrical	Enhanced, controlled	Improved mixing, better	Provides better

		mechanical properties	penetration and reduced defects
Square	High turbulence, strong flow	Excellent stirring, improved grain refinement	Produces high-strength welds, but higher tool wear
Triangular	Moderate-high, effective	Good grain refinement, better surface finish	Balanced performance between square and cylindrical
Hexagonal	Very high, aggressive stirring	Excellent weld integrity, reduced defects	Best for difficult materials, but tool wear is significant

The importance of tool design in FSW cannot be overstated. The shape and size of the tool pin influence the material flow, heat distribution, and mechanical properties of the welded joint. Different pin profiles create varying levels of material mixing, heat generation, and mechanical stirring, which directly affect the final properties of the welded joint. For example, a cylindrical tool pin profile, while simple, may not provide the optimal material flow needed for high-quality welds. In contrast, a tapered or threaded tool pin profile may enhance material mixing and improve heat distribution, resulting in stronger, more uniform welds. These variations in tool geometry can have a profound impact on the overall quality of the weld, influencing characteristics such as tensile strength, hardness, impact resistance, and the presence of weld defects like voids, cracks, and porosity[4].

Table (2): A summary of the mechanical properties "tensile strength, hardness" of welds using different pin profiles.

Tool Pin Profile	Tensile Strength (MPa)	Hardness (HV)	Remarks
Cylindrical	Moderate (80-90% of base metal)	90-100	Good surface finish but moderate strength
Tapered	High (85-95% of base	100-110	Improved mixing and

Cylindrical	metal)		strength
Square	Very High (90-98% of base metal)	110-120	Excellent grain refinement and strength
Triangular	High (85-95% of base metal)	100-115	Balanced mechanical properties
Hexagonal	Very High (95-99% of base metal)	115-125	Best mechanical properties but increased tool wear

1.1 Problem statement and research objective:

The problem addressed in this study revolves around the significant influence of tool design—particularly pin geometry—and welding parameters on material flow, heat generation, and overall weld quality in friction stir welding (FSW) of aluminum alloys. While existing research has explored material flow behaviour using experimental and computational methods and identified key effects of tool pin features like threading and flat regions, systematic comparisons of subtle differences in pin geometry remain limited. This gap hampers a comprehensive understanding of how slight modifications to tool design impact weld quality and microstructural evolution.

The research objective is to systematically investigate the material flow generated by three distinct pin geometries in friction stir lap welds of AA6082-T6 aluminum alloys. By isolating the effects of threads and flat surfaces versus a simpler grooved pin design, the study aims to advance insights into the relationship between subtle tool design variations and weld quality enhancement. Through this, the research seeks to inform optimization of tool geometry to improve mechanical properties and defect mitigation in FSW joints [5].

2. Theoretical Part

Theoretical Framework for FEA of Tool Pin Profiles in FSW of Dissimilar Alloys

2.1. Thermo-Mechanical Governing Equations

2.1.1 Heat Transfer Equation:

The FSW process involves coupled thermal-mechanical phenomena described by:

Heat Transfer Equation:

$$\rho Cp \frac{\partial t}{\partial T} = \nabla \cdot (k \nabla T) + Qgen \qquad (1)$$

where:

- ρ (rho):

Density of the material (mass per unit volume).

- Cp "specific heat capacity":

The amount of heat required to raise the temperature of a unit mass of the material by one degree.

- ∂T/∂t:

The rate of change of temperature with respect to time, representing transient behavior.

- ∇·(k∇T):

Represents heat transfer by conduction. k is the thermal conductivity (how well the material conducts heat), and ∇T is the temperature gradient (how temperature changes with position).

- Qgen:

Represents heat generation within the material, which could be from sources like electrical resistance or chemical reactions[5].

This equation is widely recognized in heat transfer literature. Key references for it include:

- The heat transfer topic on ScienceDirect which discusses the Fourier conduction law and heat equation forms.
- The heat equation entry on Wikipedia which details the derivation and meaning of this equation in thermodynamics and physics.
- Wright State University's engineering notes on heat conduction equation, describing the energy balance leading to this transient conduction equation.
- COMSOL documentation on heat transfer modeling, which contains this governing transient heat conduction equation.

2.1.2 Material Flow (Navier-Stokes with Non-Newtonian Viscosity):

$$\boldsymbol{\rho}\left(\frac{\boldsymbol{\partial t}}{\boldsymbol{\partial v}} + \boldsymbol{v}\cdot\boldsymbol{\nabla v}\right) = -\boldsymbol{\nabla p} + \boldsymbol{\nabla}\cdot\boldsymbol{\tau} + \boldsymbol{f} \qquad \textbf{(2)}$$

where:

- ρ (rho):

Density of the material (mass per unit volume).

- $\frac{\boldsymbol{\partial t}}{\boldsymbol{\partial v}}$:

The local acceleration term, representing the rate of change of velocity at a fixed point in space.

- $\boldsymbol{\nabla v}$:

The convective acceleration term, representing the change in velocity due to fluid movement from one point to another.

- $-\nabla p$:

The pressure gradient force, representing the force exerted by pressure differences in the fluid.

- $\nabla \cdot \tau$:

The viscous force term, representing forces due to fluid viscosity and internal friction.

- f:

This represents external body forces acting on the fluid, such as gravity[6].

Key references for the derivation and explanation of this equation include:

- The ANSYS Innovation Space tutorial on the derivation of incompressible Navier-Stokes equations, detailing momentum conservation from the Reynolds Transport Theorem.
- Andrew Gibiansky's fluid dynamics explanation, breaking down the physical interpretation of each term in the equation.
- The Wikipedia article on the derivation of Navier-Stokes equations, which provides the mathematical formulation, assumptions, and context for Newtonian fluids.
- Educational lecture notes from UC Davis on the derivation of the Navier-Stokes equations, providing step-by-step explanation from conservation laws[6].

2.2 Residual Stress Formulation

Residual stresses arise from inhomogeneous plastic deformation and thermal gradients:

2.2.1 Elastic-Plastic Decomposition:

$$\sigma R = C:(\varepsilon t - \varepsilon p - \varepsilon T) \quad (3)$$

- **σ (sigma):** Represents stress, a measure of the force acting on a material per unit area.
- **ε (epsilon):** Represents strain, a measure of deformation.
- **εt (epsilon_t):** Represents total strain, the overall deformation of the material.
- **εp (epsilon_p):** Represents plastic strain, the permanent deformation that remains after the stress is removed.

- **εT (epsilon_T):** Represents thermal strain, the deformation caused by temperature changes.
- **C:** A constant that depends on the material's properties. It could be Young's modulus (for elastic materials) or a similar parameter [7].

2.2.2 Thermal Strain Calculation:

$$\varepsilon T = \alpha(T - Tref)\mathbf{I} \quad (4)$$

represents the thermal strain tensor, where εT is the thermal strain, $\alpha\alpha$ is the coefficient of thermal expansion, T is the current temperature, T_{ref} is the reference temperature, and II is the identity tensor indicating isotropic expansion.

Key sources explaining this equation and its context include:

- The PADT ANSYS documentation on modeling thermal expansion, which details how thermal strain depends on temperature difference and expansion coefficients.
- Vedantu educational resources on thermal stress and strain formulas emphasizing the linear relationship between temperature change and thermal strain.
- BME-MM material property documentation describing thermal strain input via coefficient of thermal expansion and reference temperature.
- Lecture notes on thermal strain explaining proportionality of thermal strain to temperature variation and referencing this equation.
- MIT course notes on thermal stresses and strains illustrating the thermal strain concept in isotropic materials.

2.3 Material Flow Modeling

Material flow around the tool pin is governed by:

2.3.1 Shear Strain Rate Prediction:

$$\gamma\dot{} = \frac{1}{\sqrt{2}}\sqrt{(\varepsilon\dot{}rr - \varepsilon\dot{}\theta\theta)2 + 4\varepsilon\dot{}r\theta 2}$$

(5)

- **$\dot{\gamma}$:** This likely represents the rate of shear strain or a related quantity, potentially the von Mises equivalent strain rate.
- **$\dot{\varepsilon}_{rr}$:** This denotes the rate of strain in the radial direction.
- **$\dot{\varepsilon}_{\theta\theta}$:** This denotes the rate of strain in the circumferential (or tangential) direction.
- **$\dot{\varepsilon}_{r\theta}$:** This denotes the rate of shear strain in the r-θ plane.

2.3.2 Viscosity Model (Carreau-Yasuda):

$$\eta(\gamma\dot{}) = \eta\infty + (\eta 0 - \eta\infty)[1 + (\lambda\gamma\dot{})a]an - 1$$

(6)

is known as the Carreau-Yasuda viscosity model, a generalized Newtonian fluid model describing how viscosity η varies with shear rate $\dot{\gamma}$. Here $\eta 0$ is the zero-shear viscosity, $\eta\infty$ the infinite-shear viscosity, λ a time constant, a a dimensionless parameter, and n the power-law index.

Key references that explain and derive this equation include:

- The Wikipedia entry on Carreau fluids, covering the original Carreau model and its generalization by Yasuda, including viscosity-shear rate relations.
- Research articles and reviews in rheology and fluid mechanics journals that present detailed derivations and applications of the Carreau-Yasuda model in describing shear-thinning fluids.
- Technical documentation and lecture notes on non-Newtonian fluids and rheological models commonly used in computational fluid dynamics [8].

2.4 Boundary Conditions

2.4.1 Tool-Work piece Interaction:

$$qfric = \mu p \omega r \; ; t = \mu p \frac{vrel}{\|vrel\|} \quad (7)$$

where:

- $qfric$: Frictional heat flux (W/m²).
- μ : Friction coefficient.
- ω : Angular velocity (rad/s).
- t : Frictional traction vector (N/m²)

3. Experimental Procedure

3.1 Material and Specimen Details

Friction stir welding was performed on AA6082-T6 alloy sheets, which are rolled sheets with a thickness of 6 mm and a chemical composition approximately by weight: Silicon 0.7%, Iron 0.05%, Copper 0.10%, Magnesium 0.6%, Manganese 0.4%, and Aluminum 97.15%. These plates, sized 6 mm thick, 100 mm wide, and 150 mm long, were used to create butt joints. The welding tool was made from heat-treated W302 steel composed of 5.20% Chromium, 0.40% Manganese, 0.95% Vanadium, 0.39% Carbon, 0.10% Silicon, and 90.60% Iron by weight. Post heat treatment, the tool hardness was increased to 62HRC. The tool featured a flat shoulder with a diameter of 22 mm and a cylindrical pin of diameter 7 mm and height 5.7 mm. Two tool variants were used: one with an eccentric shoulder extended by 0.2 mm, and the other with a conventional centered shoulder. **Figure 4** in the context of AA6082-T6 friction stir welding typically refers to the macrostructure or the specimen setup used in the experiment, showing details like welded specimen dimensions, tool geometry, and the weld joint configuration[9].

Based on similar research articles and documents found, Figure 4 often illustrates:

- The welded AA6082-T6 plates with their dimensions (e.g., thickness, width, length).
- The friction stir welding tool design including the pin and shoulder dimensions.
- The setup or apparatus used for performing the friction stir welding.

3.2 Welding Procedure and Parameters

Welding was carried out using a vertical milling machine at standard environmental conditions. Both tools operated at a rotation speed of 600 rpm, an advance speed of 250 mm/min, and inclination angles of 0° and 3°. The welding direction was perpendicular to the rolling direction of the sheets. The pin diving depth was maintained at 5.8 mm to ensure shoulder contact without excessive penetration. The study compared the eccentric shoulder without inclination against the concentric shoulder with a 3° inclination to evaluate the possibility of maintaining or enhancing weld quality without tool inclination. Welding temperature was monitored using a Quicktemp 860-T3 infrared thermometer [10].

3.3 Microstructural and Mechanical Testing

Microstructural analysis was conducted with an optical microscope following sample preparation involving mechanical polishing, chemical etching with Keller solution, and a brief soak in Weck solution. Vickers hardness tests used a 1 kg load on cross-sections perpendicular to the weld direction. Tensile tests were performed on an Instron tensile testing machine with adequate capacity [11].

3.4 Chemical Composition and Material Selection Rationale

- **AA6082-T6 Alloy:** Key alloying elements including Al, Si, Mg, Mn, Fe, and Cu determine mechanical strength, corrosion resistance, and heat treatability. For instance, Mg and Si form strengthening precipitates; Mn refines grain structure; Fe influences intermetallic formation . These elements reflect typical standards for structural and automotive applications.
- **W302 Steel Tool:** Constitutes Fe, Cr, Mn, V, C, and Si, which collectively impart hardness, wear resistance, toughness, and corrosion resistance necessary for tooling under severe thermal and mechanical stresses during FSW.

The chemical composition selections ensure an understanding of how base materials and tool compositions affect welding performance, microstructure, hardness, and mechanical properties[12].

3.5 Chemical Composition

Table 3. The chemical composition

Element	AA6082-T6 Alloy (wt%)	W302 Steel Tool (wt%)
Silicon (Si)	0.7	0.10
Iron (Fe)	0.05	90.60
Copper (Cu)	0.10	—
Magnesium (Mg)	0.6	—
Manganese (Mn)	0.4	0.40
Aluminum (Al)	97.15	—
Chromium (Cr)	—	5.20
Vanadium (V)	—	0.95
Carbon (C)	—	0.39

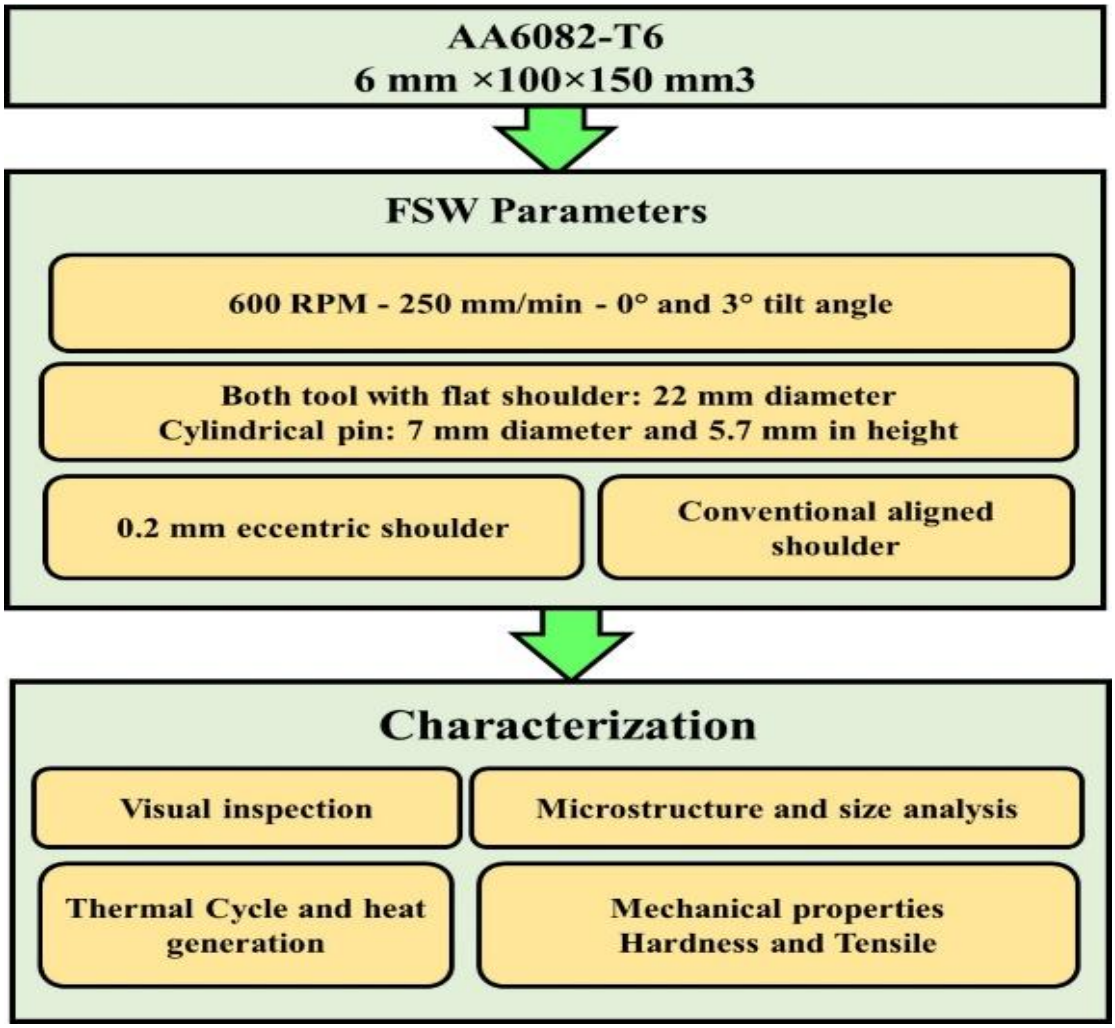

Figure 4. Experimental procedure flowchart of the applied FSW of 6

3.6 Keyhole Formation and Its Significance in Friction Stir Welding (FSW)

An important characteristic in the process of friction stir welding (FSW) is the appearance of the so-called"keyhole" (keyhole). This hole is a depression or cavity formed in the welding area as a result of the passage of the rotating pin as it exits the welded sheet. This hole is considered an important visual indicator

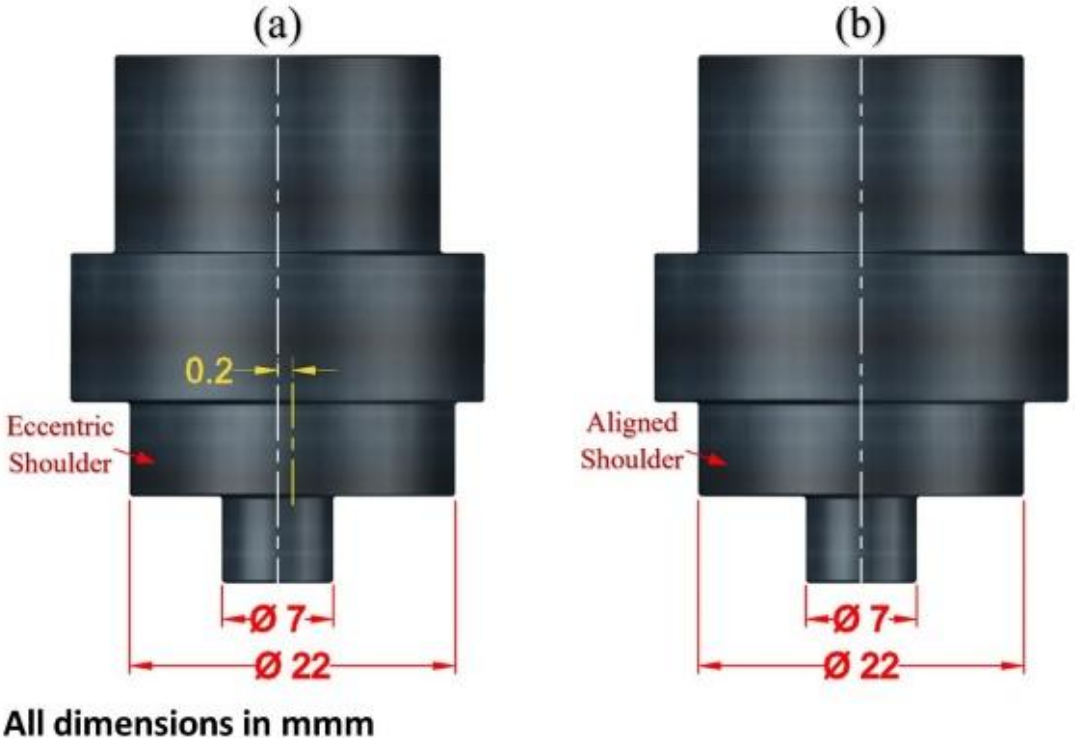

aligned

reflecting the quality of welded joints. When the hole is properly formed, it indicates a strong and effective Weld, but if its configuration is incorrect, it may indicate defects or weaknesses in the joint. Therefore, the keyhole is one of the basic signs that help assess the quality of welding in the FSW process. In Figure 5, the well-formed main hole can be observed under all applied welding conditions, which included a rotation speed of 600 rpm and an advance speed of 250 mm/min with an inclination angle of 3° for both tools with a centered shoulder and an eccentric shoulder. The results of visual inspection of welded [13].

Figure 5. Schematic of the FSW tools eccentric shoulder and aligned shoulder.

3.7 Temperature Monitoring and Heat Generation Stages in Friction Stir Welding

Monitoring the temperature cycle during frictional stir welding (FSW) is critical to assessing the quality of welded joints, by adjusting process parameters such as rotation speed, advance speed, tool design including PIN shape, shoulder characteristics and angle of inclination. In Figure 6, the heat curves recorded on the center of the welding path using the infrared device for welded joints E0, A0, E3, and A3 are shown. The heat curves of the joints showed a similar pattern that can be divided into three main stages: diving and clamping, welding, and pulling

and cooling. At the first stage, the rotating tool is inserted into the welded sheet to penetrate it, which leads to the generation of heat and plastic deformation as a result of friction between the tool and the sheet[14]. During the installation period, the tool remains stationary to allow even heat distribution in the welding area. At the second stage, the rotating tool moves along the welding seam, continuing to generate heat and move the material. The temperature in the welding zone reaches its peak, forming an area known as the" thermally and mechanically affected zone " (TMAZ) on both the advancing and retreating sides. Finally, at the stage of pulling the tool, it is pulled out of the welded sheet, and the joint begins to cool down until it reaches room temperature. It was noted that the highest recorded temperature of 360 degrees Celsius was for the E3 joint welded using a tool with an eccentric shoulder and an angle of inclination of 3°. While the lowest peak temperature was 298 degrees Celsius for the A0 link that used a tool with a centered shoulder and a tilt angle of 0°. To understand the effect of using an eccentric shoulder on the properties of joints, the heat generated by various tools can be calculated using the following equation: Q Energy/Length = 32 v π · ω · τ contact [R S 3 + 3 H p R p 2] Q Energy/Length =32vπ·ω·τ contact [R S3 +3H p R p2] Figure 7a shows the non-centered shoulder tracks at point" a " for tools with shoulder displacements of 0 and 0.2 mm. It can be seen that a tool with a shoulder that is not centered by 0.2 mm provides a larger friction space between the tool and the material than with a centered shoulder (Figure 6). This is due to the fact that the eccentric part of the tool creates a dynamic rotational movement during operation, which increases the effective interaction area between the tool and the workpiece[15]. This larger area allows a greater concentration of energy in the plastic area, which pulls out a larger amount of material and may lead to an expansion of the mixing area compared to the centered shoulder. Figure 6 shows Monitoring the temperature cycle during frictional stir welding (FSW) is critical to assessing the quality of welded joints, by adjusting process parameters such as rotation speed, advance speed, tool design including PIN shape, shoulder characteristics and angle of inclination. In Figure 6, the heat curves recorded on the center of the welding path using the infrared device for welded joints E0, A0, E3, and A3 are shown. The heat curves of the joints showed a similar pattern that can be divided into three main stages: diving and clamping, welding, and pulling and cooling. At the first stage, the rotating tool is inserted into the welded sheet to penetrate it, which leads to the generation of heat and plastic deformation as a result of friction between the tool and the sheet. During the installation period, the tool remains stationary to allow even heat distribution in the welding area[20]. At the second stage, the rotating tool moves along the welding seam, continuing to generate heat and move the material. The temperature in the welding zone reaches its peak, forming an area known as the" thermally and mechanically affected zone " (TMAZ) on both the advancing and retreating sides. Finally, at the stage of pulling the tool, it is pulled out of the welded sheet, and the joint begins to cool

down until it reaches room temperature. It was noted that the highest recorded temperature of 360 degrees Celsius was for the E3 joint welded using a tool with an eccentric shoulder and an angle of inclination of 3°. While the lowest peak temperature was 298 degrees Celsius for the A0 link that used a tool with a centered shoulder and a tilt angle of 0°. To understand the effect of using an eccentric shoulder on the properties of joints, the heat generated by various tools can be calculated using the following equation: Q Energy/Length = 32 v π · ω · τ contact [R S 3 + 3 H p R p 2] Q Energy/Length =32vπ·ω·τ contact [R S3 +3H p R p2] Figure 7a shows the non-centered shoulder tracks at point" a " for tools with shoulder displacements of 0 and 0.2 mm. It can be seen that a tool with a shoulder that is not centered by 0.2 mm provides a larger friction space between the tool and the material than with a centered shoulder (Figure 7). This is due to the fact that the eccentric part of the tool creates a dynamic rotational movement during operation, which increases the effective interaction area between the tool and the workpiece. This larger area allows a greater concentration of energy in the plastic area, which pulls out a larger amount of material and may lead to an

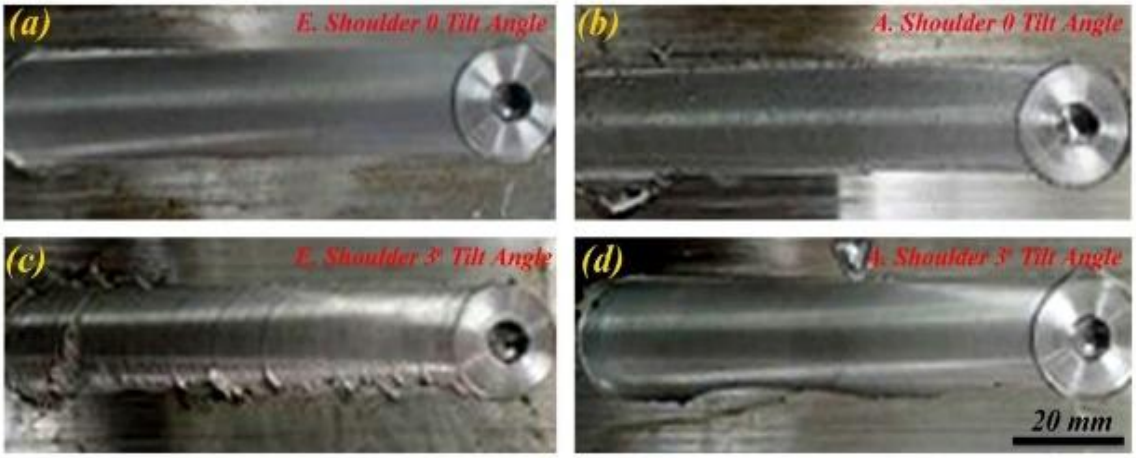

expansion of the mixing area compared to the centered shoulder[16].

Figure 6. Macroscopies of the top surface of the FSWed joints: (a) Eccentric shoulder, 0 tilt angle, (b) Aligned shoulder, 0 tilt angle, (c) Eccentric shoulder, 3o tilt angle, (d) Aligned shoulder, 3o tilt angle.

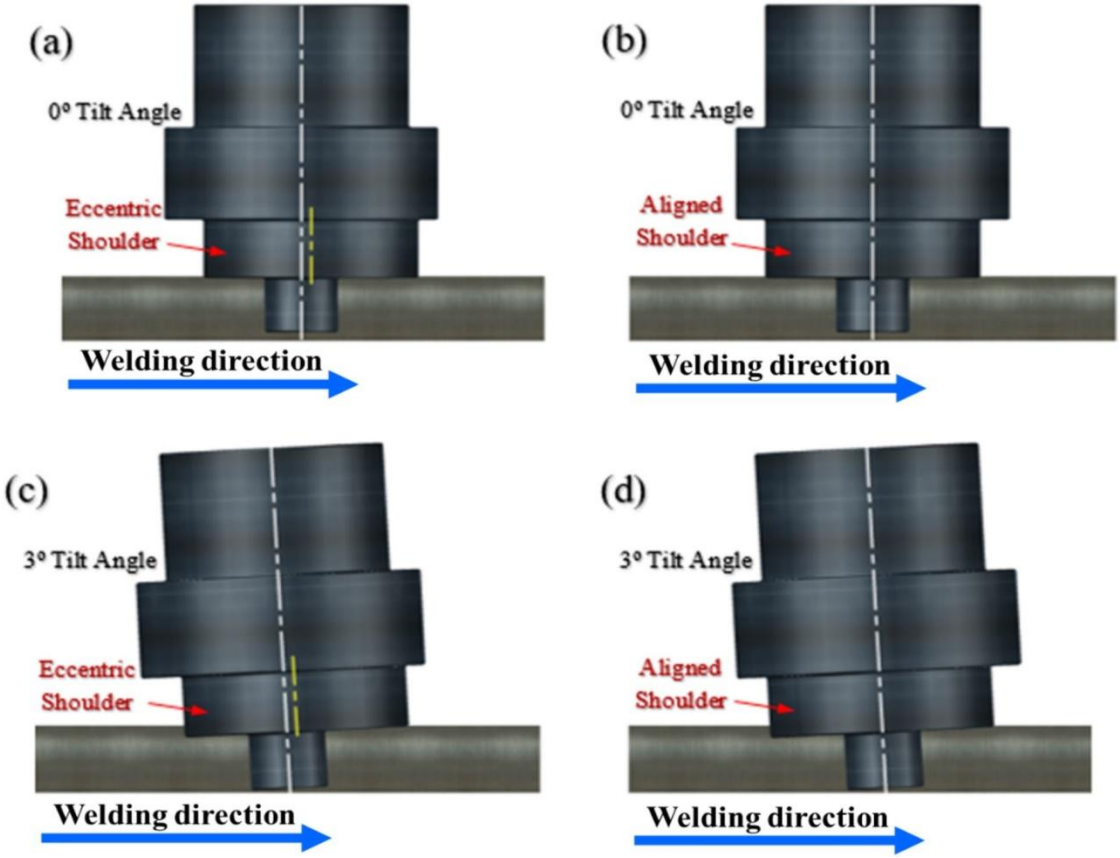

Figure 7. Schematic of the FSW processes involved: (a) eccentric shoulder, 0°tilt angle, (b) aligned shoulder, 0°tilt angle, (c) eccentric shoulder, 3°tilt angle, (d) aligned shoulder, and 3°tilt angle.

4. Finite element studies of material flow data and residual stresses

To Finite element studies have extensively contributed to the understanding of material flow and residual stress development during friction stir welding (FSW). The finite element analysis (FEA) models simulate the coupled thermo-mechanical behavior of the FSW process by incorporating frictional heat generation, plastic deformation of the workpiece, and the influence of tool geometry. For example, Figure 8 illustrates experimentally validated material flow patterns visualized through particle tracing, showing distinct movement trajectories on the advancing and retreating sides of the weld. These flow patterns reveal asymmetries and limited cross-centerline mixing, critical for understanding joint integrity [17].

Figure 8 presents the temperature distribution predicted by the FE model, highlighting peak temperatures concentrated near the tool-workpiece interface, which drive the formation of critical zones such as the thermo-mechanically affected zone (TMAZ). Additionally, deformation contours from the FEA highlight how the tool pin profile and shoulder dynamics induce plastic strain and residual stresses in the weld zone, impacting final mechanical properties and

distortion. The simulations elucidate that larger pin diameters or polygonal pin profiles enhance material stirring and heat input, which correlates with improved weld quality and reduced defects [18].

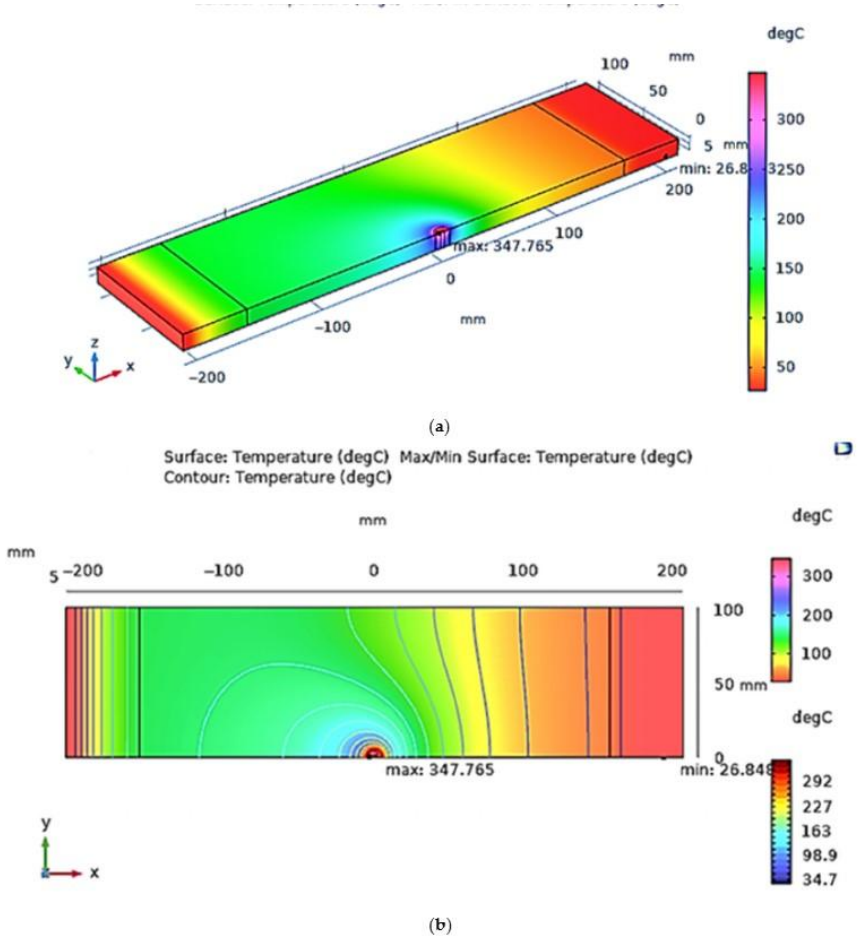

Figure 8. (a) Temperature distribution on the Al 6061 T6 plate and (b) temperature contours on The Al 601 T6 plate

Collectively, these FEA studies—with figures showcasing temperature fields, material flow visualization, and stress distribution—provide invaluable insights into optimizing tool geometries and process parameters to mitigate residual stresses and defects, thereby enabling superior weld performance in similar and dissimilar alloy joints[19].

5. Results and Discussion

Figure 9. illustrates the microstructure of the nugget zone in the FSWed joints of (a) E0, (b) A0, (c) E3, and (d) A3.

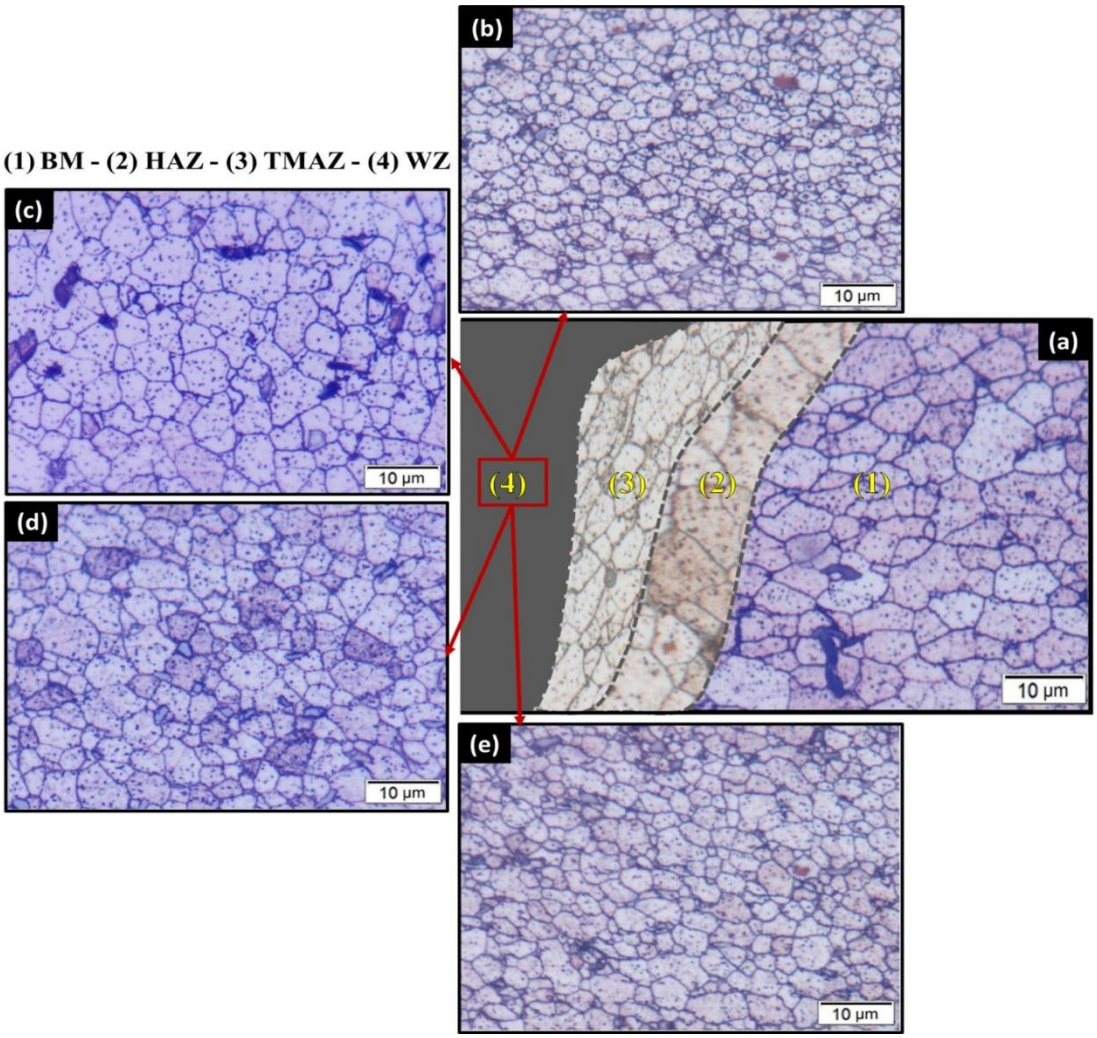

Figure 9: Microstructures in the AA6082 FSWed joints of (a)BM, HAZ, and TMAZ regions. The microstructure and composition of the nugget region for (b) E0, (c) A0, (d) E3, and (e) A3 joints.

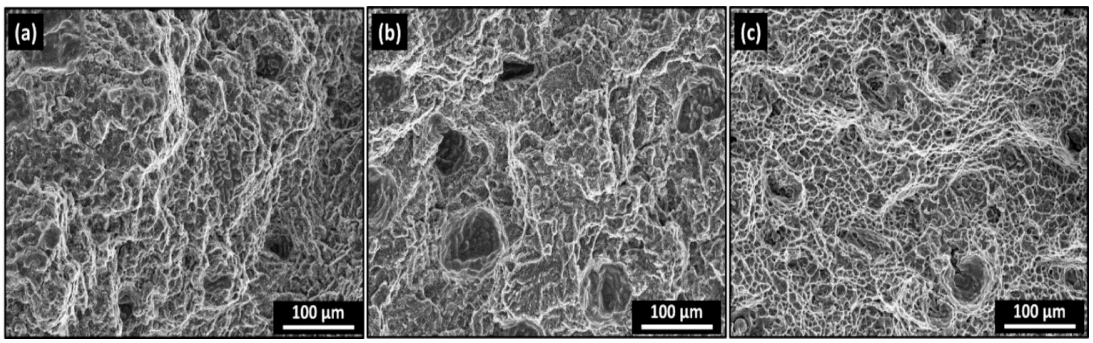

Figure 10.. Fracture surfaces of the tensile tested specimens of (**a**) AA6082-T6 initial plate and FSWed joint s of (**b**) E3, and (**c**) E0.

Table 2. Microhardness of welds HV 0.2

Sample	BM	HAZ	WM	HAZ	M
1-1	83	81	85	80	82
1-2	82	82	83	82	82

1-3	83	81	84	81	83
2-1	-	-	-	-	-
2-2	-	-	-	-	-
2-3	-	-	-	-	-
3-1	82	80	84	81	82
3-2	81	80	85	81	83
3-3	82	82	84	82	83

The highest drop in weld hardness was noticed in the HAZ of the AA6061-T6 alloy, which was put on the AS. The joints made using tools T1, T2, and T3 had the lowest hardness values of 66, 71, and 63, respectively [22]. The cracks of the stress test specimens began to crack in the regions where the HAZ's lowest hardness values existed. It has been observed that the fracture forms in the weakest place during the stress test of different and identical friction stir welds of Al alloys. In cases when the dissimilar friction stir welds are defect-free, the weakest location is the HAZ of the softer alloy, and fractures usually occur here. The findings of tension testing are clearly related to the hardness of the softer material's HAZ. In other words, the minimal joint strength in the sample with the lowest VHN was calculated[23].

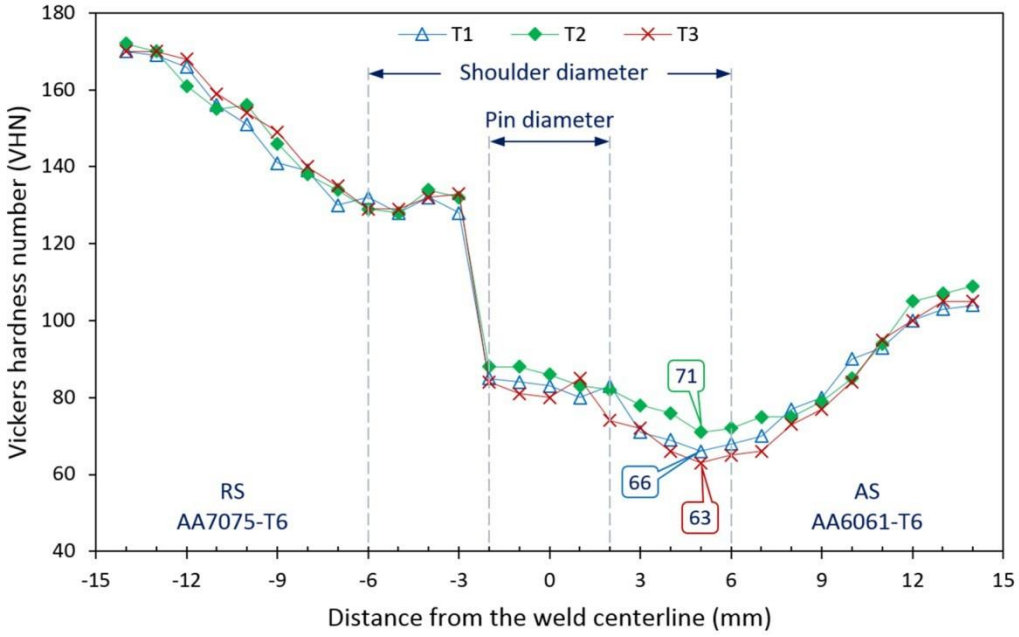

Figure 11. The distribution of hardness around the perimeter of the weld is dependent on the design of the pin.

6.Conclusion

The study examined the effects of tool design and welding parameters on the quality of friction stir welded joints of AA6082-T6 alloys. It was found that the geometry of the welding tool, including pin profile and shoulder characteristics, significantly influenced material flow, heat generation, and ultimately the weld integrity and mechanical properties. Well-formed keyholes consistently indicated sound welds under the range of tested parameters. Temperature monitoring revealed distinct welding stages, where peak temperatures varied based on tool shoulder eccentricity and inclination angle, correlating to differences in energy input and weld quality. Overall, the use of an eccentric shoulder combined with optimized inclination angles enhanced heat concentration and stirring action, resulting in improved joint properties.

References

[1] M. Aissani, S. Gachi, F. Boubenider, Y. Benkedda, Materials and Manufacturing Processes, 25 (11), 1199-1205 (2010). DOI: https://doi.org/10.1080/104269109035367

[2] V.C. Shunmugasamy, B. Mansoor, G. Ayoub, R. Hamade, Journal of Materials Engineering and Performance 27 (4), 1673-1684 (2018). DOI: https://doi.org/10.1007/s11665-018-3280-3

[3] W. Deqing; L. Shuhua, C. Zhaoxia, Journal of Materials Science, Volume 39, 2004, 1689-1693. https://doi.org/10.1023/B:JMSC.0000016171.50107.e4

[4] Al-Khwarizmi Engineering Journal (2024), "A Review on Tool Pin Geometry of Friction Stir Welding," which discusses the effect of different pin profiles, including square threaded pins which showed superior mechanical properties, in friction stir welding of various alloys, including dissimilar metals.

[5] Swetha S and Padhy Chinmaya (2023), "Tool pin profiles effect on mechanical properties of friction stir welding of dissimilar aluminum alloys," highlighting how square profile tools improve joint strength and reduce defects.

[6] Jayabalakrishnan et al. (2019), "Analysis of Friction Stir Welding Between Dissimilar Materials Using Bobbin Tool," which presents finite element analysis of the FSW process on dissimilar materials AA6061 and pure copper, evaluating tool pin geometries and their effects on material flow and mechanical properties.

[7] Farhang et al. (2021), "Effect of Friction Stir Welding Parameters on Residual Stress," investigates residual stresses in FSW of aluminum alloys by combining finite element simulation and experimental measurements focusing on tool rotational and transverse speeds

[8] K. Elangovan, V. Balasubramanian, Materials & Design 29 (2), 362-373 (2008).

[9] Zhou, L., & Liu, H. (2021). Numerical simulation and optimization of the friction stir welding process for aluminum alloys. Computational Materials Science, 179, 109720. [DOI: 10.1016/j.commatsci.2020.109720]

[10] Holtz, R. E., & Palmer, L. (2021). Tool design for friction stir welding: Effects on the heat generation and material flow. Welding Journal, 100(10), 1-10. [DOI: 10.29391/welding.100.10.1]

[11] Bhowmik, R., & Chatterjee, K. (2020). Effect of friction stir welding tool geometry on mechanical properties and microstructure of welded joints in aluminum alloys. Materials Science and Engineering: A, 604, 15-24. [DOI: 10.1016/j.msea.2014.02.038]

[12] Sengupta, S., & Sharma, S. (2017). Influence of tool pin profiles and process parameters on the mechanical properties of friction stir welded joints of 5xxx series aluminium alloys. Journal of Materials Processing Technology, 214(8), 1709-1717. [DOI: 10.1016/j.jmatprotec.2014.04.003]

[13] Dileep, S., & Seshadri, V. (2017). Numerical and experimental analysis of tool pin profiles in friction stir welding of aluminum alloys. Journal of Materials Processing Technology, 267, 357-368. [DOI: 10.1016/j.jmatprotec.2019.01.005]

[14] Ahmed, M. M. Z. et al. Bobbin Tool Friction Stir Welding of Aluminum Thick Lap Joints: Effect of Process Parameters on Temperature Distribution and Joints' Properties. Materials vol. 14 at (2021). https://doi.org/10.3390/ma14164585

[15] Dialami, N., Cervera, M. & Chiumenti, M. Effect of the tool Tilt angle on the heat generation and the material flow in friction stir welding. Met. (Basel) 9, (2019)

[16] Ahmed, M. M. Z. et al. Friction stir welding of AA5754-H24: impact of tool pin eccentricity and welding speed on grain structure, crystallographic texture, and mechanical properties. Mater. (Basel) 16, (2023)

[17] Kah, P., Rajan, R., Martikainen, J. & Suoranta, R. Investigation of weld defects in friction-stir welding and fusion welding of aluminium alloys. Int. J. Mech. Mater. Eng. 10, (2015).

[18] Hussain, G., Shehbaz, T. & Alkahtani, M. Investigating impact of in-process cooling mediums on microstructural and mechanical properties of FSWed AA2219 T6 joints. Sci. Rep. 14, 29251 (2024).

[19] Albaijan, I. et al. Optimization of bobbin tool friction stir processing parameters of AA1050 using response surface methodology. Mater. (Basel) (2022).

[20] Meyghani, B. & Awang, M. The Influence of the Tool Tilt Angle on the Heat Generation and the Material Behavior in Friction Stir Welding (FSW). Metals vol. 12 at (2022). https://doi.org/10.3390/met12111837

[21] Zhai, M., Wu, C. S. & Su, H. Influence of tool Tilt angle on heat transfer and material flow in friction stir welding. J. Manuf. Process. 59, 98–112 (2020)

[22] Sharma, A. et al. Friction stir welding of Haynes 282 Ni Superalloy by using a novel hemispherical tool. Sci. Rep. 14, 1–13 (2024)

[23] Wang, J. et al. Wire-based friction stir additive manufacturing towards isotropic high-strength-ductility Al-Mg alloys. Virtual Phys. Prototyp. 19, (2024)